

Layered semiconductor devices with water top-gates: High on-off ratio field-effect transistors and aqueous sensors

Yuan Huang,¹ Eli Sutter,² and Peter Sutter,^{3*}

¹*Institute of Physics, Chinese Academy of Sciences, Beijing, 100190, China*

²*Department of Mechanical & Materials Engineering, University of Nebraska-Lincoln, Lincoln, NE 68588, USA*

³*Department of Electrical & Computer Engineering, University of Nebraska-Lincoln, Lincoln, NE 68588, USA*

Abstract

Layered semiconductors show promise as channel materials for field-effect transistors (FETs). Usually, such devices incorporate solid back or top gate dielectrics. Here, we explore de-ionized (DI) water as a solution top gate for field-effect switching of layered semiconductors including SnS₂, MoS₂, and black phosphorus. The DI water gate is easily fabricated, can sustain rapid bias changes, and its efficient coupling to layered materials provides high on-off current ratios, a near-ideal sub-threshold swing, and enhanced short-channel behavior even for FETs with thick, bulk-like channels. Screening by the high-k solution gate eliminates hysteresis due to surface and interface trap states and substantially enhances the field-effect mobility. The onset of water electrolysis sets the ultimate limit to DI water gating at large negative gate bias. Measurements in this regime show promise for aqueous sensing, demonstrated here by the amperometric detection of glucose in aqueous solution. DI water gating of layered semiconductors can be harnessed in research on novel materials and devices, and it may with further development find broad applications in microelectronics and sensing.

*Corresponding author, e-mail: psutter@unl.edu

Keywords: Field-effect transistor, layered semiconductors, tin disulfide, molybdenum disulfide, black phosphorus.

Significance Statement

Layered semiconductors show promise as channel materials for field-effect transistors (FETs), but due to screening and limited field penetration the solid gate dielectrics usually employed in such devices can only control the conductance of ultrathin FET channels. Here we explore solution gating of layered FETs using de-ionized water as a gate dielectric. The DI water gate couples strongly to the channel, provides hysteresis free high on-off ratio switching, high carrier mobility and enhanced short-channel behavior even for FETs with thick, bulk-like channels. Water-gated FETs lend themselves naturally to aqueous sensing, demonstrated here by sensitive glucose detection. DI water gating of layered semiconductors can be harnessed in research on novel materials and devices, as well as broad applications in microelectronics and sensing.

Introduction

Field-effect transistors (FET), especially those made of silicon, play a central role in microelectronics (1, 2). Layered crystals, such as graphite, MoS₂, SnS₂, WS₂ and others whose electronic structure has long been known (3-10) have only recently been considered as channel materials for FET devices (11-14). One important reason is that although several layered semiconductors have sizable bandgaps, carrier transport in thick, bulk-like crystals could not be modulated effectively by electrical fields due to screening and the resulting limited penetration of the gate electric field. The successful isolation of single-layer graphene opened new possibilities for field-effect devices by demonstrating that the carrier density in atomically thin devices can be tuned by moderate applied electric fields, even in semimetals (15). Graphene FETs have shown very high carrier mobilities of up to 10⁶ cm²/Vs, but the vanishing bandgap limits their application in digital logic because graphene transistors cannot be turned off, i.e., show large off-state currents (16). This limitation of graphene has led to efforts to exfoliate layered semiconductors, for example transition metal dichalcogenides such as MoS₂, to singlelayer thickness for field-effect devices and the exploration of the fundamental properties of such monolayer semiconductors (11, 13, 17, 18). The on-off ratio in MoS₂ FETs, for example, reaches up to 10⁸ at room temperature (11) and other 2D semiconductors (WS₂, WSe₂, SnS₂, etc.) showed similar values, as well as a host of other fascinating properties (19-25).

Previous studies of layered semiconductor FETs have mainly focused on single- and few-layer devices, with nearly all reports to date involving channel thicknesses below 10 layers (11, 12). The interest in the ultrathin limit is in part driven by emerging properties due to the extreme carrier confinement in 2D crystals, but also reflects shortcomings of conventional gating strategies in controlling the conductance of thicker device channels. Back gating via a thick SiO₂ dielectric, the prevalent way of modulating electronic transport in studies of novel 2D and layered materials, offers relatively poor gate coupling and field penetration into layered crystals and hence cannot turn off devices with thicker, bulk-like channels. Top gates can achieve higher electric fields, but are more difficult to fabricate and still offer limited control over the conductance of thick FETs. Ionic liquids (26, 27) can be used to achieve very large electric fields in 2D and layered materials (28), sufficient for example to induce

superconductivity in MoS₂ (29, 30). But ionic liquid gates face practical limitations. Slow charge transfer processes, for instance, require low bias scan rates to maintain equilibrium at the gate-channel interface. This calls for the development of alternative gating methodologies to study charge transport in layered materials and to harness the inherent advantages of FETs with thicker channels (31-34) compared to ultrathin single- or few-layer devices: higher current carrying capacity; lower Schottky barriers and hence reduced contact resistance at the layered semiconductor/metal junction (35, 36); and relative insensitivity to thickness fluctuations of the active layer, which facilitates robust, high-yield device fabrication over large areas.

Here, we explore the use of a de-ionized (DI) water top gate (13) for field-effect tuning of the conductance of thick layered-semiconductor FETs. This approach offers an alternative route toward efficient layered field-effect devices: instead of reducing the channel thickness to the ultimate 2D limit, the conductance of a thicker channel is switched between on- and off-states by a gate that supports very large electric fields at the channel surface. We find that the field penetrates sufficiently deep into the bulk that high on-off current ratios (up to 10⁷) can be obtained for device channels up to several hundred layers thick. In addition, the efficient gating implies that short-channel effects can be largely suppressed even for thicker channels. Since liquid gate drops are simply dispensed onto the semiconductor surface and contacted by a suitable electrode, the fabrication challenges of solid top-gate dielectrics are avoided. Gating via the double layer at the water-semiconductor interface supports much higher voltage sweep rates than ionic liquids. Finally, the use of an aqueous solution for gating provides facile access to water-based sensing, which we demonstrate here by detecting glucose with high sensitivity down to concentrations below 1 mM. While we focus mainly on FETs with layered tin disulfide (SnS₂, a n-type semiconductor with ~2.3 eV bandgap, (13)) channels to illustrate the characteristics of DI water top gates, the approach is generally applicable to a broader class of layered semiconductors with inert as well as more reactive surfaces, as demonstrated for devices with thick MoS₂ and black phosphorus channels.

Results and Discussion

Figure 1 illustrates the layout of the FET devices used here. The active channel consists of a layered semiconductor such as SnS₂, here prepared by exfoliation from highquality bulk

crystals to a typical thickness of 50-60 nm (~80-100 layers) and supported on 300 nm SiO₂/Si. The contacts (Ti/Au, 5 nm/50 nm, see Methods for details) are covered by a thin polymer (poly-methyl methacrylate, PMMA) layer to electrically isolate them from the gate, which consists of a DI-water drop applied by pipette. The device can be gated alternatively by a top-gate voltage (VTG) applied to an electrode in contact with the water drop, or by back gating (V_{BG}) via the SiO₂ support (Fig. 1a). Figs. 1 b-e show cross-sectional transmission electron microscopy (TEM) images of one of the fabricated devices (without the PMMA insulator layer). The active region, ~82 nm thick, is mostly homogeneous but shows a number of stacking faults and embedded smaller rains. In higher magnification TEM images, the layered structure is clearly visible (Fig. c, d) with periodicity of ~0.6 nm (Fig. 1e), consistent with the layer spacing of SnS₂ (13).

A direct comparison of the transfer characteristics of devices with back- and solution top gating demonstrates the striking effects due to the high electric fields at the water/layered metal dichalcogenide interface. The electric field applied via the SiO₂ back gate fails to bring the thick (~80 nm) SnS₂ channel into its off state, even for large applied voltages (-20 V, Fig. 2a). This is evidenced by a poor on-off current ratio (~10 over a wide range, $-20 \leq V_{BG} \leq 20$ V), as well as large “off-state” source-drain currents, I_{SD} (Fig. 2b). The same device controlled by DI-water top gate shows substantially improved transconductance characteristics. I_{SD} is now efficiently modulated via small changes in gate bias, $|V_{TG}| < 1$ V (Fig. 2c) and the channel is efficiently turned off, as demonstrated by on-off ratios exceeding 10^5 (Fig. 2d). These values are sufficient for practical, low voltage operation of layered metal chalcogenide-based field-effect devices. Similar behavior is observed for other materials. Fig. 3 shows examples of device characteristics of FETs with thick MoS₂ and black phosphorus channels. As for SnS₂, a comparison of back-gating via the 300 nm SiO₂/Si support with top-gating by DI water shows significantly enhanced on-off ratios with the solution gate, even for channels with thickness of several tens of nanometers.

Top-gating by DI-water not only enhances the field penetration of thick device channels, allowing them to be turned off completely, but it also improves the current hysteresis during gate bias sweeps and results in a substantially higher carrier mobility. These improvements are illustrated in Fig. 4 for SnS₂ field-effect transistors. FETs fabricated from layered

materials often show significant hysteresis, assigned primarily to charge trapping by surface and interfacial trap states (37). As can be seen in Fig. 4a, the transfer characteristic of back-gated SnS₂ devices indeed shows this hysteresis upon reversal of the gate bias sweep direction. The on-off ratio of this device is 67 over a gate voltage range from -35 to +40 V, and similar to the FET shown in Fig. 2 it cannot be turned off completely. When controlled by DI-water top gate, the same device shows almost no detectable hysteresis upon reversal of the gate voltage sweep direction (Fig. 4b), which implies that charge traps are no longer active after the water drop is applied. This behavior is consistent with the absence of surface adsorbates in the solution environment and an effective screening of interface states by the high-k dielectric ($\epsilon_{\text{rel}}(\text{H}_2\text{O}) \sim 80$). Qualitatively similar results have also been reported for thin MoS₂ FETs employing HfO₂ or Al₂O₃ top gates (38-40). Again, solution top gating causes a striking enhancement of the on-off ratio to 5×10^5 , nearly four orders larger than with the back gate and results in a near-ideal sub-threshold swing of 80 mV/decade (Fig. 4b). To compare the field-effect electron mobility for the two gate types, the mobility has been calculated from the transconductance characteristics via $\mu = \frac{dI_{SD}}{dV_G} \cdot \frac{L}{WC_{VSD}}$. The particular transistor considered in Fig. 4 had an aspect ratio $L/W = 3$, and the gate capacitance is either $C(\text{SiO}_2) = 11.6 \text{ nF/cm}^2$ (back gate, (41)) or $C(\text{H}_2\text{O}) = 137 \text{ nF/cm}^2$ (top gate), the double-layer capacitance of the DI water gate in contact with a SnS₂ FET channel determined previously (13). The field effect mobility increases from $50 \text{ cm}^2/\text{Vs}$ (back gated) to $180 \text{ cm}^2/\text{Vs}$ (top gated). This increase due to screening of scattering centers by the liquid dielectric is less pronounced than in the case of thinner few-layer or monolayer SnS₂ FETs since surface and interface scatterers play a relatively smaller role in the devices with thick channel considered here. Measurements of the on-off ratio on devices with different channel thickness (Fig. 4c) demonstrate that the overall gains due to liquid gating are nearly independent of the thickness of the active layer, so that on-off current ratios greater than 10^5 can be maintained for bulk-like channels up to at least 200 nm in thickness.

Layered semiconductors may offer superior scaling and improved short-channel characteristics compared with silicon FETs. We fabricated FETs with channel length ranging from 2 μm to 200 nm to compare the scaling of SnS₂ FETs with SiO₂ back gate and DI-water top gate (Fig. 5a). Devices with thin ($\sim 8 \text{ nm}$) and long channel show consistently high on-off

ratios ($>10^6$), both controlled by back gating and solution top gating. However, for channel length below ~ 800 nm the on-off ratio of back-gated devices drops below 10^5 whereas that of the top-gated devices remains high (Fig. 5b). A similar trend is observed for FETs with thick (55 nm) SnS₂ channel (Fig. 5c). The already low on-off ratio of back-gated devices drops even further for short channels with length below 1 μm . In contrast, the on-off ratio of devices controlled by DI water top gates remains high ($\sim 10^6$) over the entire range of channel lengths considered here. This suggests that the very high electric fields achievable at the solid-liquid interface can effectively prevent possible leakage due to a finite source-drain bias at short channel lengths, so that the off-current remains low at least down to the shortest channels considered here (200 nm). This beneficial effect applies to both ultrathin devices, which have been considered extensively before (36, 42), as well as thicker, bulk-like layered semiconductor devices that are the focus of the present work. The observed trends can be understood within a framework developed for scaling in silicon, which invokes the characteristic length $\lambda = \sqrt{(\epsilon_s/\epsilon_{ox}) \cdot \tau_s \tau_{ox}}$, determined by the permittivities and thicknesses of semiconductor (ϵ_s , τ_s) and gate dielectric (ϵ_{ox} , τ_{ox}) (43). Within this picture, FETs with ultrathin channel have smaller λ , i.e., can be scaled to smaller dimensions. On the other hand, the thick devices considered here accentuate differences in short-channel effects between back- and solution top gating: reduced on-off ratio at short channel lengths for back gating, but consistently high on-off ratio with solution gating. The superior performance of the solution gate results from a combination of high permittivity ($\epsilon \sim 80$) and small thickness ($\sim 5\text{-}10$ nm) of the double-layer gate. Our results therefore suggest that the combination of a solution top gate with a relatively inert layered semiconductor active region, which forms a stable interface with aqueous solutions, can allow harnessing the advantages of thicker FET channels while still permitting scaling to short channel lengths.

We now explore in more detail the properties of the DI-water top gate itself, in particular the possibility of current flow through the gate electrode (i.e., gate leakage). The gate current I_G in top-gated SnS₂ devices was measured simultaneously with I_{SD} as the top gate bias V_G was swept for different applied source-drain voltages, V_{SD} . Representative results of these measurements are shown in Fig. 6a. The FET transconductance characteristics at different V_{SD} reflect the same behavior observed for other devices (e.g., Fig. 1), i.e., efficient control of

I_{SD} by the solution gate. Whereas the device is clearly in its off state for gate bias between -0.2 V and -1.0 V, the current starts to increase again for larger negative V_G . The measurements shown in Fig. 6a indicate that this behavior is not due to ambipolar conduction that has been reported previously for some layered semiconductors, such as bulk and ultrathin WSe_2 (17, 44). For example, the magnitude of I_{SD} is independent of source-drain bias, in contrast with the expected behavior for ambipolar FETs. Simultaneous measurements of the gate current show the same onset of increased current for $V_G \sim -1.0$ V, mirroring the behavior observed in I_{SD} . Hence, we attribute the apparent rise of I_{SD} to a rapidly increasing current flow across the gate junction at large negative bias. Note that for positive V_G there is consistently only a small amount of gate leakage, limited to $\sim 10\%$ of I_{SD} for small V_{SD} (20 mV) and below 3% of I_{SD} for larger V_{SD} (80 mV).

Further analysis (see below) shows that I_G increases asymptotically to large values at an applied bias of (-1.21 ± 0.05) V, close to the standard potential for electrolysis of water (-1.23 V). This suggests that the onset of electrolysis sets an ultimate limit to the operating range of a DI water top gate; the SnS_2 cathode (the FET channel) appears to act as a remarkably efficient electrocatalyst that facilitates water electrolysis with minimal over potential. Highly reproducible characteristics of the miniature electrochemical cell in our DI water top-gated SnS_2 FETs (Fig. 6a) raise the possibility that the gate current could be used for aqueous sensing. In the simplest case it should be possible to detect the presence of ionic solutes via an increase in conductivity across the solution gate. Here, we demonstrate a less straightforward example of aqueous sensing, the measurement of the concentration of glucose – a non-ionic solute – in water.

Fig. 6b shows I_G - V_G characteristics for different glucose concentrations $[C_6H_{12}O_6]$ in the DI water gate drop. A stepwise increase in $[C_6H_{12}O_6]$ causes well-defined changes in the I_G - V_G curves close to the onset of electrolysis. To quantify these changes, the measured data were fitted by an empirical function $I_G = I_0/(V_G - V_0)$, which correctly represents the strongly increasing (i.e., essentially diverging) gate current at the electrolysis potential (V_0). The fit results are shown as lines in Fig. 6b and summarized in Fig. 6c. According to the analysis, the change in glucose concentration affects only the current amplitude (I_0) but not the asymptotic electrolysis potential (V_0), which remains constant for all values of $[C_6H_{12}O_6]$ probed here

(0–50 mM). I_0 rises logarithmically with increasing glucose concentration (Fig. 6c). This behavior can form the basis for a simple amperometric scheme to measure glucose concentration, which is detected via the gate current I_G at any fixed gate bias near the electrolysis threshold ($V_G \leq -0.9$ V). As shown in Fig. 6d, any choice of $V_{G\text{Sense}}$ in this range will give the same logarithmic dependence of I_G on $[C_6H_{12}O_6]$, with a detection limit below 1 mM and high sensitivity in the concentration range corresponding to physiological glucose levels in human blood (~4–6.5 mM). We note that although our data show the ability to sense glucose via an electrical signal in SnS₂-based FETs, additional work is needed to probe the specificity to a single solute in the presence of other species in an aqueous solution. The incorporation of additional enzymatic components, e.g., glucose oxidase used in conventional sensors (45), may be required to achieve specific sensing. Beyond the static gate solutions used here, one can foresee the integration of SnS₂ devices in microfluidic platforms for realtime electrical sensing of aqueous solutes.

Conclusions

We have demonstrated solution gating by deionized water as a method for achieve field effect control over the conductance of a wide range of layered semiconductors, including SnS₂, MoS₂, and black phosphorus. The efficient coupling and large electric field of the solution gate provides high on-off current ratios, a near-ideal sub-threshold swing, and enhanced short-channel behavior even for bulk-like channels with thickness of several 10 nm to well over 100 nm. Other advantages of the solution top gate include facile fabrication compared to conventional approaches involving solid dielectrics, and the capability of applying rapid changes in gate bias unlike ionic liquid gates that require slow bias ramps. Screening of surface and interface trap states by the high-k solution gate eliminates the gate-bias hysteresis found for back-gated devices and substantially enhances the field-effect mobility. These favorable characteristics of DI water gating in FETs can readily be leveraged in materials and device research, and they may find applications in microelectronics if suitable encapsulation strategies for a liquid gate can be identified. The onset of water electrolysis and associated leakage currents sets the ultimate limit to DI water gating at large negative gate bias. Measurements in this regime show promise for aqueous sensing, explored here by the amperometric detection of glucose in static drops down to concentrations of ~1 mM. By incorporating layered semiconductor FETs into microfluidic platforms, this approach

could be expanded to allow high-throughput sensing in aqueous solutions.

Acknowledgements

This work was supported by the U.S. Department of Energy, Office of Science, Basic Energy Sciences, under Award No. DE-SC0016343. Device fabrication was carried out at the Center for Functional Nanomaterials, which is a U.S. DOE Office of Science Facility, at Brookhaven National Laboratory under Contract No. DE-SC0012704.

Methods

1. Sample preparation.

Adhesive tape was used to exfoliate layered bulk crystals (SnS₂, MoS₂, black phosphorus). It was folded 2-3 times to make the bulk crystal thinner. The tape with SnS₂ (or other layered material) was put onto the surface of a SiO₂/Si (300 nm) substrate cleaned by oxygen plasma. Before peeling off the adhesive tape, the substrate together with layered crystal/tape was put on a hot plate to anneal for 1-2 min at 100 °C to improve the contact area between the layered crystal and SiO₂ surface and obtain large flakes (46).

2. Device fabrication and electrical measurements.

After transfer of SnS₂ (or MoS₂, black phosphorus) flakes to SiO₂/Si substrate by mechanical exfoliation, optical microscopy was used to identify selected flakes with different thickness; the thickness was measured by AFM. Photoresist was spin-coated onto the substrates (S1811, 3000 rpm, 1 min), and annealed on a hot plate at 110°C for 2 min. Patterning was done using UV lithography (mask aligner Karl Suss, MA6), followed by resist developing in solvent. Ti/Au (5 nm/50 nm) contact metallization was performed in a lift-off process by e-beam evaporation, followed by photoresist dissolution in acetone. The devices were annealed in ultrahigh vacuum (10⁻⁹ Torr) to enhance the contact resistance. Electrical measurements were performed on a four-probe station (Signatone). For DI water top-gated FETs, an additional PMMA layer was deposited on the devices, baked at 180°C for 2 min., and patterned by electron-beam lithography to open windows for contact between the water drops and the device channel.

3. Transmission electron microscopy on complete devices.

Fully functional FET devices were covered in platinum and prepared into electron

transparent cross-section specimens by focused ion beam (FIB) milling using a FEI Helios dual beam FIB instrument, followed by transfer to TEM grids. The FIB sections included the device channel and the adjacent source and drain contacts. TEM imaging was performed in a FEI Tecnai Osiris ChemiSTEM microscope at 200 kV beam energy.

References

1. Kuhn KJ (2012) Considerations for ultimate CMOS scaling. *IEEE Trans. Electron Devices* 59(7):1813-1828.
2. Ferain I, Colinge CA, & Colinge J-P (2011) Multigate transistors as the future of classical metal-oxide-semiconductor field-effect transistors. *Nature* 479(7373):310-316.
3. Slonczewski JC & Weiss PR (1958) Band Structure of Graphite. *Phys Rev* 109(2):272-279.
4. Carter JL & Krumhansl JA (1953) Band Structure of Graphite. *J Chem Phys* 21(12):2238-2239.
5. Kasowski RV (1973) Band-Structure of MoS₂ and NbS₂. *Phys Rev Lett* 30(23):1175-1178.
6. Mattheis Lf (1973) Energy-Bands for 2H-NbSe₂ and 2h-MoS₂. *Phys Rev Lett* 30(17):784-787.
7. Fong CY & Cohen ML (1972) Electronic Energy-Band Structure of SnS₂ and SnSe₂. *Phys Rev B* 5(8):3095-3101.
8. Aymerich F, Meloni F, & Mula G (1973) Pseudopotential Band-Structure of Solid-Solutions SnS_xSe_{2-x}. *Solid State Commun* 12(2):139-141.
9. Uchida SI & Tanaka S (1978) Optical Phonon Modes and Localized Effective Charges of Transition-Metal Dichalcogenides. *J Phys Soc Jpn* 45(1):153-161.
10. Greenaway DL & Nitsche R (1965) Preparation and optical properties of group IV–VI 2 chalcogenides having the CdI₂ structure. *J Phys Chem Solids* 26(9):1445-1458.
11. Radisavljevic B, Radenovic A, Brivio J, Giacometti V, & Kis A (2011) Single-layer MoS₂ transistors. *Nat Nanotechnol* 6(3):147-150.
12. Ovchinnikov D, Allain A, Huang YS, Dumcenco D, & Kis A (2014) Electrical Transport Properties of Single-Layer WS₂. *Acs Nano* 8(8):8174-8181.
13. Huang Y, *et al.* (2014) Tin Disulfide-An Emerging Layered Metal Dichalcogenide Semiconductor: Materials Properties and Device Characteristics. *Acs Nano* 8(10):10743-10755.
14. Kim BJ, *et al.* (2010) High-Performance Flexible Graphene Field Effect Transistors with Ion Gel Gate Dielectrics. *Nano Lett* 10(9):3464-3466.
15. Novoselov KS, *et al.* (2004) Electric field effect in atomically thin carbon films. *Science* 306(5696):666-669.
16. Schwierz F (2010) Graphene transistors. *Nat Nanotechnol* 5(7):487-496.
17. Das S & Appenzeller J (2013) WSe₂ field effect transistors with enhanced ambipolar characteristics. *Appl Phys Lett* 103(10).
18. Huang Y, *et al.* (2013) An innovative way of etching MoS₂: Characterization and mechanistic investigation. *Nano Res* 6(3):200-207.
19. Matte HSSR, *et al.* (2010) MoS₂ and WS₂ Analogues of Graphene. *Angew Chem Int Edit* 49(24):4059-4062.
20. Zhao WJ, *et al.* (2013) Evolution of Electronic Structure in Atomically Thin Sheets of WS₂ and WSe₂. *Acs Nano* 7(1):791-797.
21. Su GX, *et al.* (2015) Chemical Vapor Deposition of Thin Crystals of Layered Semiconductor SnS₂ for Fast Photodetection Application. *Nano Lett* 15(1):506-513.
22. Zeng HL, Dai JF, Yao W, Xiao D, & Cui XD (2012) Valley polarization in MoS₂ monolayers by optical pumping. *Nat Nanotechnol* 7(8):490-493.

23. Lee HS, *et al.* (2012) MoS₂ Nanosheet Phototransistors with Thickness-Modulated Optical Energy Gap. *Nano Lett* 12(7):3695-3700.
24. Sie EJ, *et al.* (2015) Valley-selective optical Stark effect in monolayer WS₂. *Nat Mater* 14(3):290-294.
25. Jones AM, *et al.* (2013) Optical generation of excitonic valley coherence in monolayer WSe₂. *Nat Nanotechnol* 8(9):634-638.
26. Chao S & Wrighton MS (1987) Solid-state microelectrochemistry: electrical characteristics of a solid-state microelectrochemical transistor based on poly(3-methylthiophene). *Journal of the American Chemical Society* 109(7):2197-2199.
27. Panzer MJ, Newman CR, & Frisbie CD (2005) Low-voltage operation of a pentacene field-effect transistor with a polymer electrolyte gate dielectric. *Appl Phys Lett* 86(10):103503.
28. Misra R, McCarthy M, & Hebard AF (2007) Electric field gating with ionic liquids. *Appl Phys Lett* 90(5):052905.
29. Ye JT, *et al.* (2012) Superconducting Dome in a Gate-Tuned Band Insulator. *Science* 338(6111):1193-1196.
30. Costanzo D, Jo S, Berger H, & Morpurgo AF (2016) Gate-induced superconductivity in atomically thin MoS₂ crystals. *Nat Nanotechnol*.
31. Zhang YW, *et al.* (2016) Thickness Considerations of Two-Dimensional Layered Semiconductors for Transistor Applications. *Sci Rep-Uk* 6.
32. Li SL, *et al.* (2014) Thickness Scaling Effect on Interfacial Barrier and Electrical Contact to Two-Dimensional MoS₂ Layers. *Acs Nano* 8(12):12836-12842.
33. Kim S, *et al.* (2012) High-mobility and low-power thin-film transistors based on multilayer MoS₂ crystals. *Nat Commun* 3.
34. Bao WZ, Cai XH, Kim D, Sridhara K, & Fuhrer MS (2013) High mobility ambipolar MoS₂ field-effect transistors: Substrate and dielectric effects. *Appl Phys Lett* 102(4).
35. Mak KF, Lee C, Hone J, Shan J, & Heinz TF (2010) Atomically Thin MoS₂: A New Direct-Gap Semiconductor. *Phys Rev Lett* 105(13).
36. Liu H, Neal AT, & Ye PDD (2012) Channel Length Scaling of MoS₂ MOSFETs. *Acs Nano* 6(10):8563-8569.
37. Late DJ, Liu B, Matte HSSR, Dravid VP, & Rao CNR (2012) Hysteresis in Single-Layer MoS₂ Field Effect Transistors. *Acs Nano* 6(6):5635-5641.
38. Chang HY, *et al.* (2013) High-Performance, Highly Bendable MoS₂ Transistors with High-K Dielectrics for Flexible Low-Power Systems. *Acs Nano* 7(6):5446-5452.
39. Zeng L, *et al.* (2013) Remote phonon and impurity screening effect of substrate and gate dielectric on electron dynamics in single layer MoS₂. *Appl Phys Lett* 103(11).
40. Radisavljevic B, Whitwick MB, & Kis A (2011) Integrated Circuits and Logic Operations Based on Single-Layer MoS₂. *Acs Nano* 5(12):9934-9938.
41. Farmer DB, Lin YM, & Avouris P (2010) Graphene field-effect transistors with self-aligned gates. *Appl Phys Lett* 97(1).
42. Du YC, Liu H, Deng YX, & Ye PD (2014) Device Perspective for Black Phosphorus Field-Effect Transistors: Contact Resistance, Ambipolar Behavior, and Scaling. *Acs Nano* 8(10):10035-10042.
43. Yan RH, Ourmazd A, & Lee KF (1992) Scaling the Si Mosfet - from Bulk to Soi to Bulk. *Ieee T Electron Dev* 39(7):1704-1710.
44. Podzorov V, Gershenson ME, Kloc C, Zeis R, & Bucher E (2004) High-mobility field-effect transistors based on transition metal dichalcogenides. *Appl Phys Lett* 84(17):3301-3303.
45. Heller A & Feldman B (2008) Electrochemical glucose sensors and their applications in diabetes management. *Chemical reviews* 108(7):2482-2505.
46. Huang Y, *et al.* (2015) Reliable Exfoliation of Large-Area High-Quality Flakes of Graphene and Other Two-Dimensional Materials. *Acs Nano* 9(11):10612-10620.

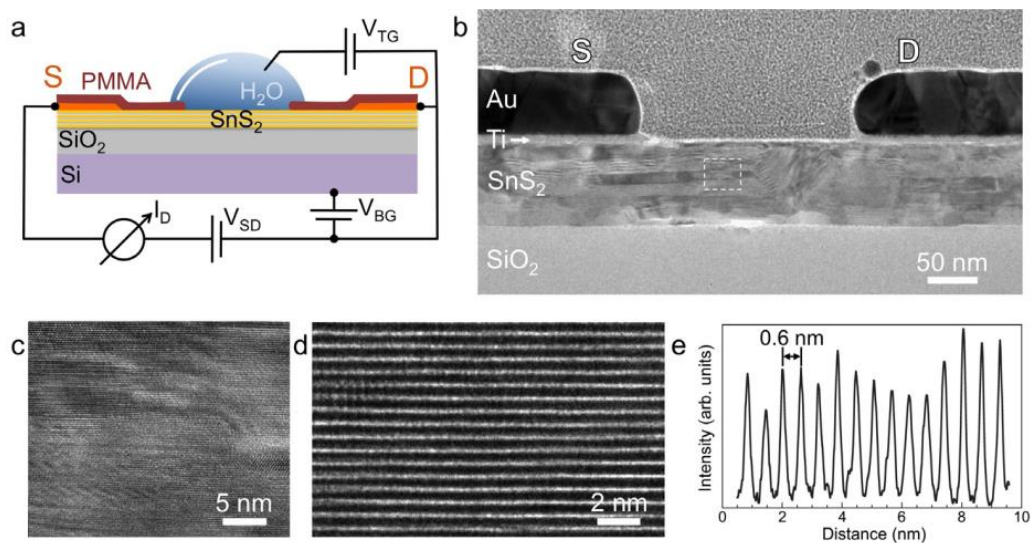


Figure 1. Schematic and cross-sectional TEM of a field-effect transistor (FET) with multilayer SnS₂ channel. **a.** Schematic geometry of layered metal chalcogenide semiconductor based devices (e.g., with SnS₂ channel). S: Source electrode; D: Drain; V_{BG}: Back-gate voltage, applied via the SiO₂/Si substrate; V_{TG}: Top-gate voltage, applied via a de-ionized water solution gate, insulated by PMMA from the source/drain contacts. **b.** TEM image of a FET device with 80 nm thick SnS₂ channel (~210 nm channel length) and Au/Ti contacts, supported on SiO₂/Si. **c.** High-magnification view of the region of the SnS₂ channel marked in a. **d.** High-resolution TEM image, showing the SnS₂ layering. **e.** Line profile showing a layer spacing of ~0.6 nm in the SnS₂ FET channel.

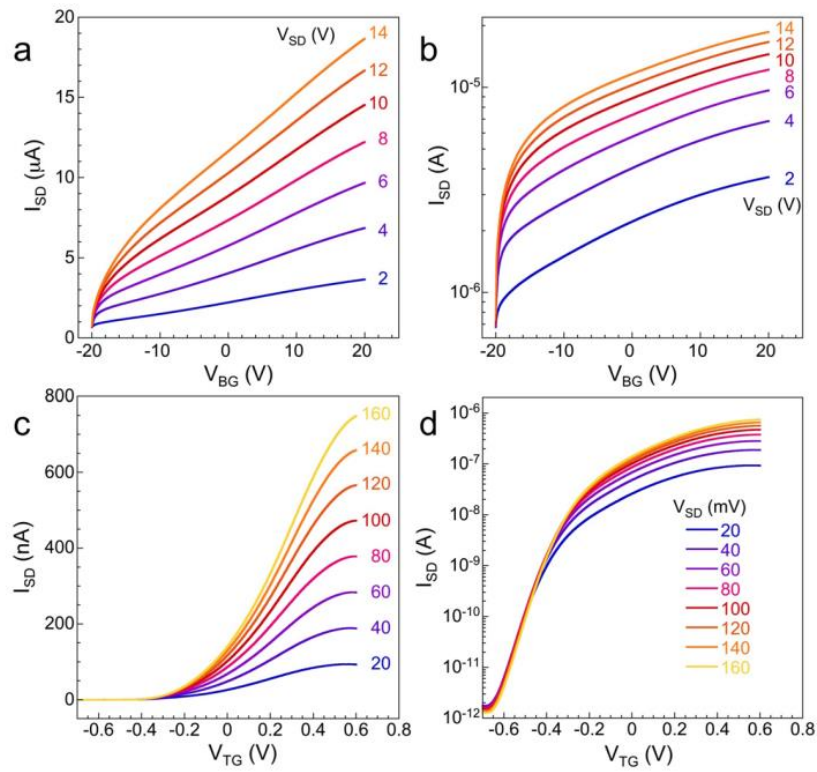


Figure 2. Device characteristics of a thick (~80 nm) SnS₂ FET device. **a.** Linear and **b.** logarithmic plots of the I_{SD} - V_G transfer characteristics of the back-gated FET for source-drain bias V_{SD} ranging from 2 to 14 V. For back-gate voltages between -20 - 20 V, the on-off ratio is less than 10. **c.** Linear and **d.** logarithmic plots of the I_{SD} - V_G transfer characteristics of the solution top gated FET for source-drain bias curves at low bias V_{SD} ranging from 20 to 160 mV. For top-gate voltages between -0.6 – 0.6 V the on-off ratio exceeds 10^5 .

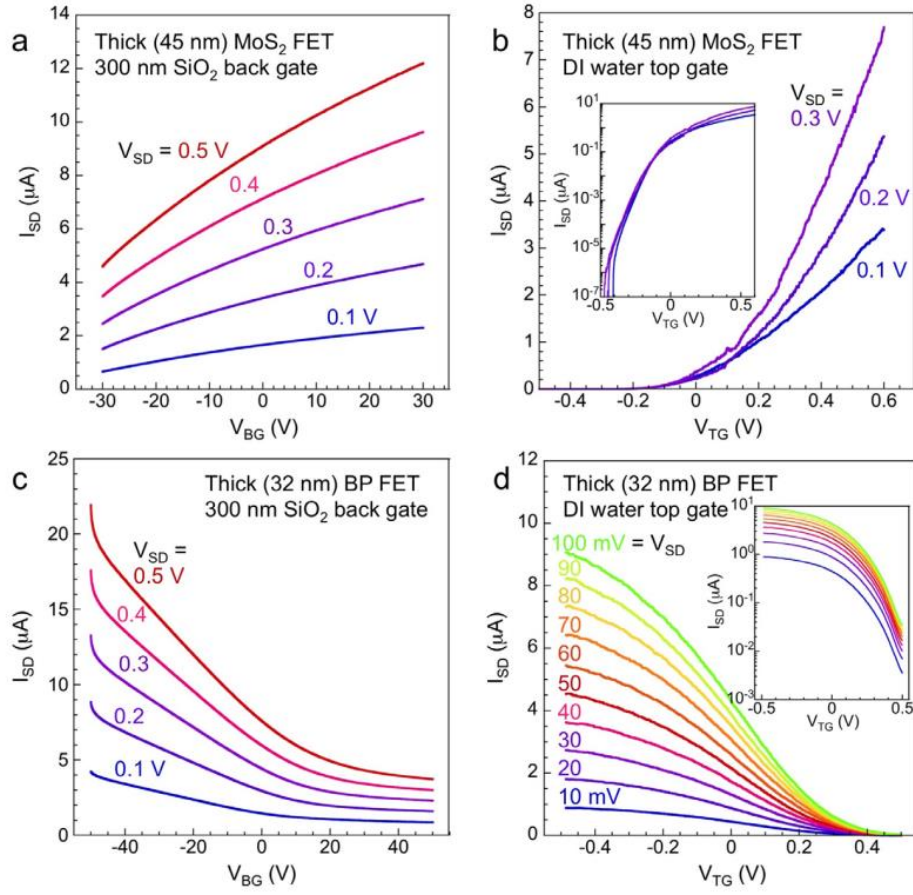


Figure 3. Characteristics of thick MoS₂ and black phosphorus FETs. **a.** I_{SD} - V_G transfer characteristics of a back-gated MoS₂ FET with 45 nm channel thickness for source-drain bias V_{SD} ranging from 0.1 V to 0.5 V. The back-gate is unable to bring the device into the off-state. **b.** Transfer characteristic of the same MoS₂ FET controlled by a DI water top gate. The logarithmic plot given in the inset shows an on-off ratio of $\sim 10^8$ of the top-gated device. **c.** I_{SD} - V_G transfer characteristics of a back-gated black phosphorus (BP) FET with 32 nm channel thickness for source-drain bias V_{SD} ranging from 0.1 V to 0.5 V. **d.** Transfer characteristic of the same black phosphorus FET controlled by a DI water top gate (V_{SD} between 10 mV and 100 mV. Inset: logarithmic representation), showing reduced off-state current of the solution-gated device.

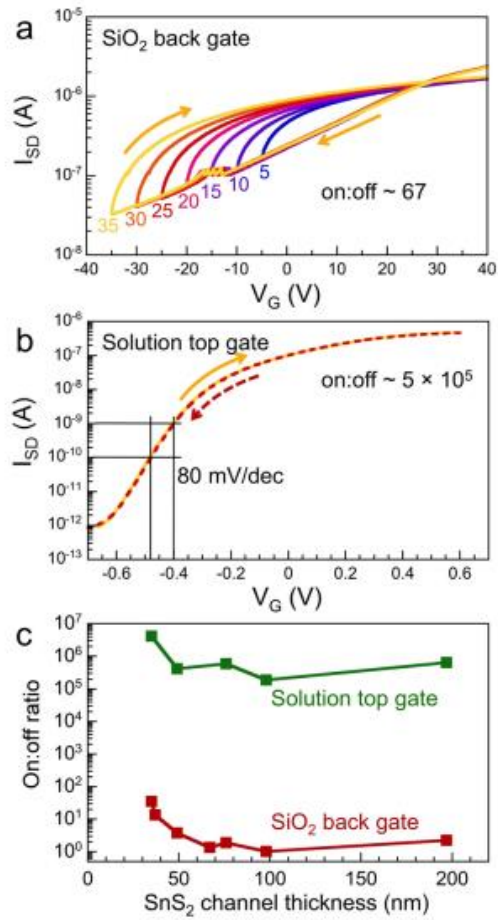


Figure 4. Hysteresis and dependence of on:off current ratio on channel thickness for SnS₂ FETs. a. Transfer characteristics of the back-gated FET, scanned from +40 V to negative gate voltages between -5 V and -35 V. Note the significant hysteresis as the V_G sweep direction is reversed, and the small on:off current ratio. **b.** Transfer characteristic of the same device with water top-gating. Note the absence of hysteresis, large on:off current ratio ($\sim 5 \times 10^5$), and nearideal sub-threshold swing (80 mV/decade). **c.** Comparison of the on:off current ratios as a function of channel thickness for devices controlled by back gating and solution top gating.

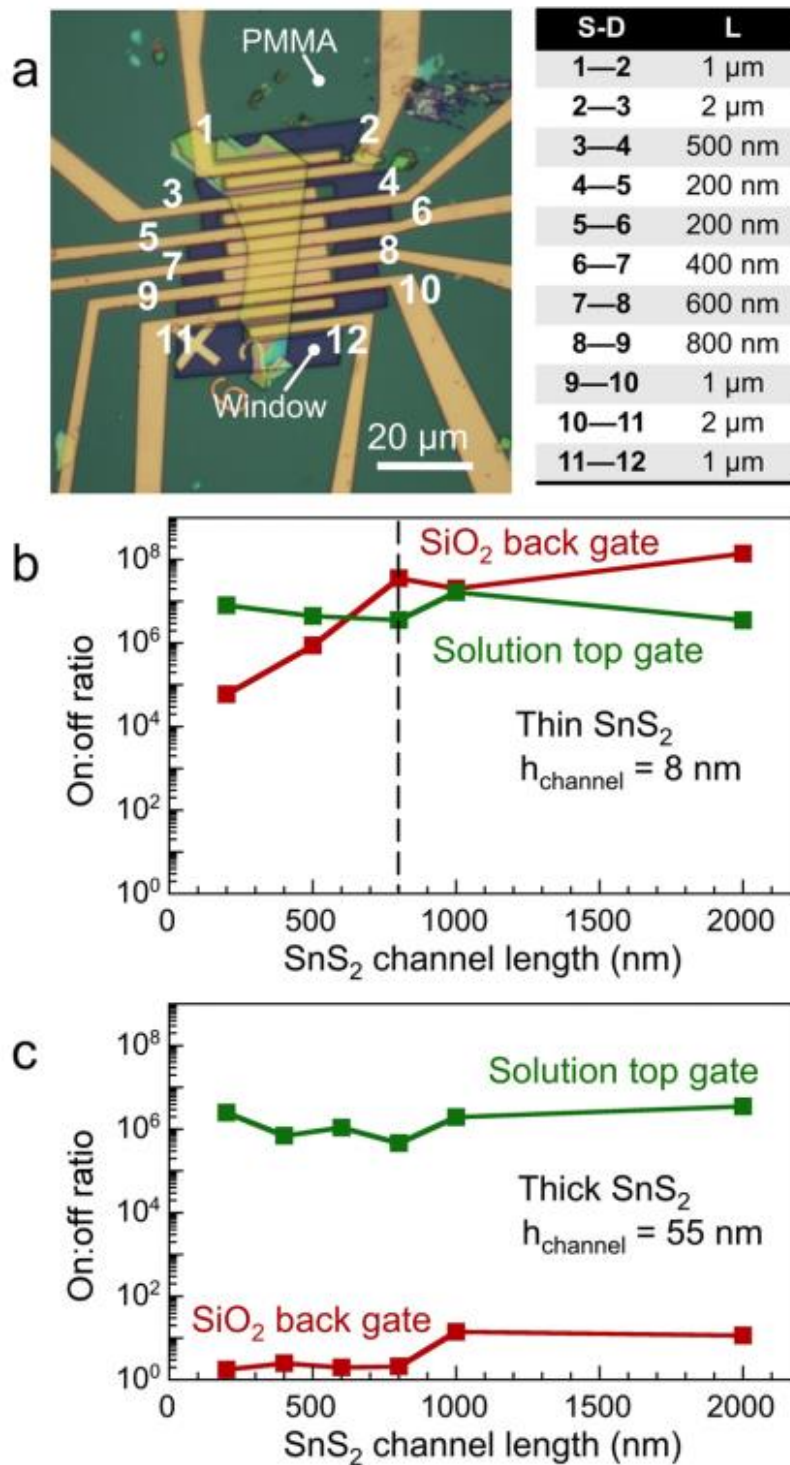


Figure 5. Short-channel effects as reflected in the on:off ratio. a. Device layout of SnS₂FETs with different channel lengths ranging from 200 nm to 2 μm . **b.** Channel length scaling for SnS₂ devices with thin (8 nm, ~13 layers) channel. **c.** Channel length scaling for SnS₂ devices with thick (55 nm) channel.

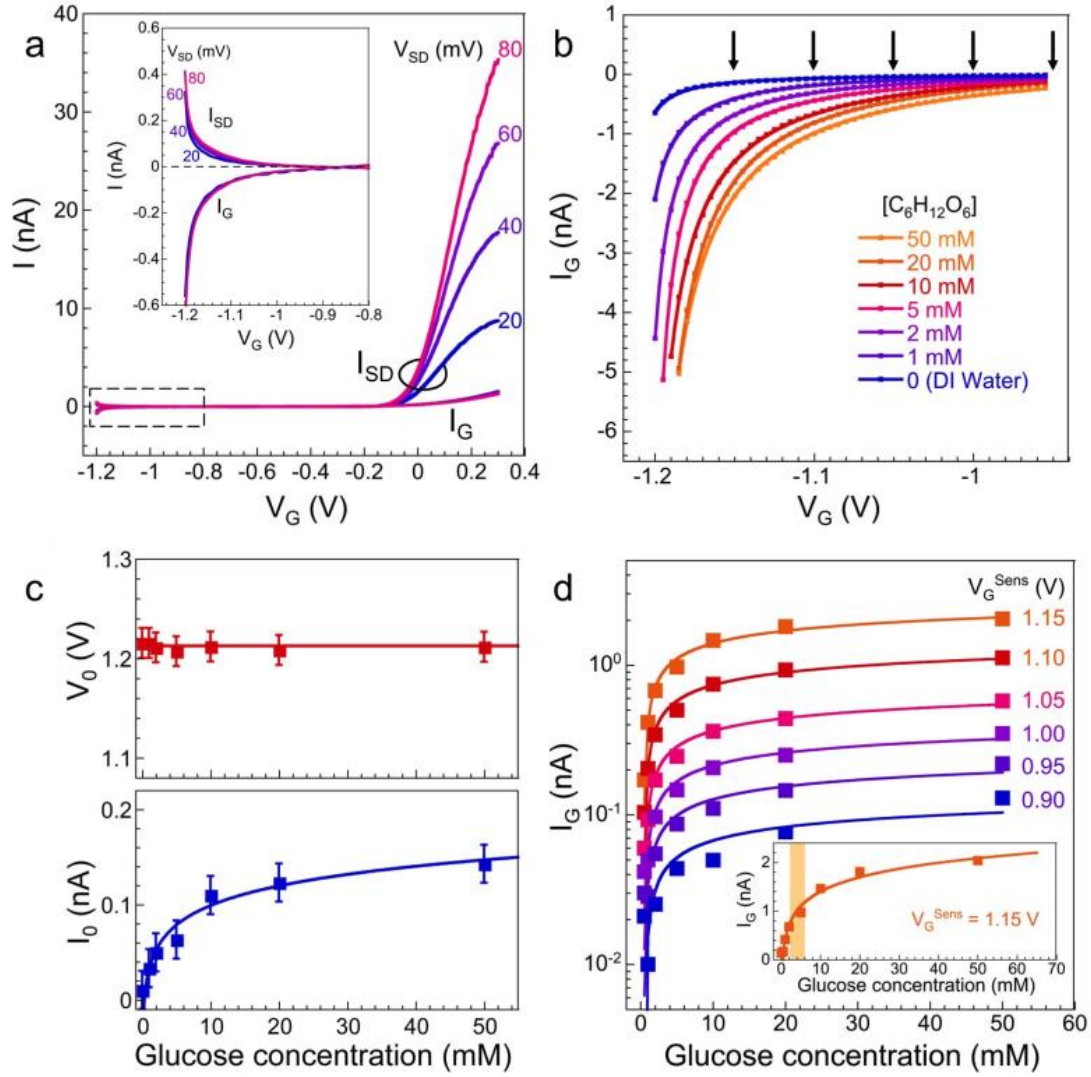


Figure 6. Gate current and its use for aqueous sensing. **a.** Source-drain current (I_{SD}) and gate current (I_G) of a FET with thick SnS₂ channel as a function of gate bias, applied to the DI water top gate. The zone of increasing I_G at large negative gate voltage, marked by a dashed rectangle, is shown at higher magnification in the inset. **b.** Change in gate current with increasing concentration of glucose in the DI water gate. Lines are fits of $I_0/(V_G - V_0)$ to the data. **c.** Summary of the fit parameters derived from **b**, showing a constant asymptote voltage V_0 but logarithmically increasing current amplitude I_0 (solid blue line: log fit) with increasing glucose concentration. **d.** Glucose sensing via the gate current, I_G , at different fixed gate voltages (labeled; also indicated by arrows in **b**). Lines are logarithmic fits to the data. The inset indicates a detection limit below 1.0 mM glucose concentration.